Piotr J. Ziółkowski,[a,b*] Wojciech Witkowski[a], Bartosz Sobczyk[a]

Analysis of unsteady forces acting on a slender cylinder

[a] Department of Mechanics of Materials and Structures, Faculty of Civil and Environmental Engineering, Gdańsk University of Technology, Gdańsk, Poland

[b] Energy Conversion Department, Institute of Fluid Flow Machinery Polish Academy of Sciences, Fiszera 14, 80-231 Gdańsk, Poland

Abstract

Developments in construction engineering (new materials, construction techniques) facilitate the design of very flexible, light structures with low damping which unfortunately results in higher susceptibility of these structures to wind action. It is therefore necessary to use more accurate scientific tools in the engineering phase of these structures. Analytical methods for considering wind effects on structures encounter difficulties with respect to mathematical formulations of aerodynamic forces. In this paper a 2D numerical model has been described which considers the fluid domain with respect to a cylindrical obstacle. This 2D model has been discretized using the finite volume method, and numerical simulations have been undertaken in order to describe the unsteady flow conditions within the analyzed domain. The simulations have been performed with boundary conditions characterizing the flow past a cylindrical obstacle. The results have been compared with the literature data from similar experiments. On the basis of the flow characteristics obtained, as well as the spatial distributions of the flow parameters, a model for further 3D analyses was selected. Next, a 3D numerical study of unsteady flow forces acting on a slender cylinder has been analyzed. Toward the end, a two-way fluid solid interaction approach has been utilized, which incorporates a computational fluid dynamics approach combined with computational solid dynamics.

Keywords: Unsteady flow; FSI; CFD modelling; CSD modelling

*Corresponding Author. E-mail adress: pjziolkowski@imp.gda.pl

1 Introduction

Wind can cause many dangerous phenomena which can lead to the catastrophic collapse of a structure. The Tacoma Narrows Bridge disaster in 1940 and the devastation of three cooling towers at Ferrybridge in 1965 are very expressive examples of the destructive power of wind action. In the first case a flutter was the agent of destruction and aerodynamic interference in the second [1]. In design process of some structural members such as towers and masts, certain aeroelastic phenomena including vortex shedding and the lock-in phenomenon, cross-wind galloping, wake galloping, torsional divergence, flutter and buffeting have to be taken into account [1–3].

The vortex shedding phenomenon is to be considered within this paper. It was noted first by Strouhal that the so-called Bernard-Kármán vortices, being generally a pattern of alternately appearing, repeatable and swirling vortices on the leeward side of a blunt body, have their own frequency of formation, which is proportional to the wind velocity [4]. The vortex shedding phenomenon can be thus described by a similarity number, the so-called Strouhal number [5]

$$\mathrm{Sh} = \frac{a}{vt} = \frac{af}{v} \ , \tag{1}$$

where a is the characteristic dimension, v is the steady ambient velocity of the uniform flow, t is the period of tested phenomena, and $f = 1/t$ the frequency of the vortex shedding.

It should be added that the Strouhal number is used not only in civil engineering in the design processes, but is also widely applied in mechanical engineering for the purpose of different flow analyses, as for example a flow around a vibrating body (aerofoil, the rod, thermowell), flow through a blade ring seated in a rotor disc and flow around a rotating propeller or screw propeller, etc. [6].

The published papers, relating to non-stationary flows in civil engineering topics, have become more and more focused on numerical works [7–12]. These experimental studies and analyses are widely described in [8,9,13–15]. Zdravkovich has indicated that real flows around cylinders in most practical applications are exposed to many disturbances and have been quantified by a set of influencing parameters [16]. However it has been emphasized that detailed experimental data is required for the correct classifications of the parameters. The typical examples of the most frequently encountered influencing parameters include free stream turbulence, surface roughness, the wall blockage (it is observed only in experiments), small gaps between the cylinder and the flow channel walls, the aspects ratio (ratio of the height to the diameter of the cylinder) and the free end, trans-

verse and streamwise oscillations [16]. The current knowledge of the flow above
the free end of a finite-height circular cylinder, which is fixed to lateral surface at
its bottom, has been reviewed by Sumner in [17], who focuses on models of the
flow field, measurements of the local velocity field and numerical simulations.

Fluid solid interaction (FSI) or fluid structure interaction[1], is a relatively
new tool, which helps to solve physical problems involving interactions between
a structure and the fluid flow around the structure. The deformation of the struc-
ture is caused by fluid (air) flow and the behaviour of the fluid stream is affected
by the structure deformation.

Two approaches to couple the characteristics of the solid and of the fluid are
found for the purpose of the FSI analysis. The first one is the monolithic ap-
proach. Fluid and solid domains are considered in this case as one domain and
a single solver is responsible for the solution of the governing equations [18]. The
second one is named as partitioned approach [19–21]. Here the task is divided
into three subtasks referred to respectively as the fluid, the solid and the mesh.
The flow equations are solved by the computational fluid dynamics (CFD) [23]
solver and the response of the solid body is obtained by using the computational
solid dynamics (CSD) [24] solver. This solution technique is more popular among
FSI users because of the good stability conditions of the solution and calculation
economics [22].

Another classification of the FSI solution procedures depends on a mesh treat-
ment integrating the conforming mesh methods and non-conforming mesh meth-
ods. The conforming mesh methods are required to conform meshes to the inter-
face, because the interface is treated as a physical boundary condition, where the
interface location is a part of the solution. In the non-conforming mesh methods,
the interface conditions and location are set as the model constraints, so that the
fluid and the solid equations can be solved independently of each other [25].

The main focus of the paper is the 3D numerical analysis of unsteady flow
forces acting on a slender mast using two-way FSI tools.

2   Model description

2.1   The set of CFD balance equations

The four balance equation system that consists of one mass balance equation
and three momentum balance equations has been described in the papers [23,26].

---

[1]'Solid' goes into 'structure' when a body is very thin and instead of 3D finite elements a 2D
finite elements are used for discretization [6].

A general formulation of the balance equation has been used in the so-called non-indexed notation, which denotes vector $\mathbf{v} = v_i\mathbf{e}_i$ and tensor $\mathbf{t} = t_{ij}\mathbf{e}_i \otimes \mathbf{e}_j$, where $\mathbf{e}, \mathbf{e}_j$ are the versors $(i, j = 1, 2, 3)$ and the symbol $\otimes$ denotes the Kronecker product.

The set of CFD balance equations (mass and momentum conservation equation) for simulated cases is:

$$\frac{\partial}{\partial t}\left\{\begin{array}{c} \rho \\ \rho\mathbf{v} \end{array}\right\} + \mathrm{div}\left\{\begin{array}{c} \rho\left(\mathbf{v} - \mathbf{w}\right) \\ \rho\mathbf{v} \otimes \left(\mathbf{v} - \mathbf{w}\right) \end{array}\right\} = \mathrm{div}\left\{\begin{array}{c} 0 \\ \mathbf{t} \end{array}\right\} + \left\{\begin{array}{c} 0 \\ \rho\mathbf{b} \end{array}\right\} \qquad (2)$$

where: $\rho = \rho\left(\mathbf{x}, t\right)$ – fluid density, generally dependent on time t and location $\mathbf{x}$, $\mathbf{v} = v_i\mathbf{e}_i$ – fluid velocity, $\mathbf{w} = w_i\mathbf{e}_i$ – mesh velocity, $\mathbf{t} = t_{ij}\mathbf{e}_i \otimes \mathbf{e}_j$ – total stress flux, $\mathbf{b}$ – mass force of Earth gravity, $\delta_{ij} = \left\{\begin{array}{ll} 1, & i = j \\ 0, & i \neq j \end{array}\right.$ – Kronecker delta, t – the time.

Here mesh velocity $\mathbf{w}$ represents the velocity of the discretization in domain of the finite volumes. The total stress flux has been defined by

$$\mathbf{t} = -p\mathbf{I} + 2\mu\mathbf{d} - \frac{2}{3}\mu I_\mathbf{d}\mathbf{I}, \ \ \mathbf{d} = \frac{1}{2}\left(\mathrm{grad}\mathbf{v} + \mathrm{grad}^\top\mathbf{v}\right), \ \ p = \rho R T \qquad (3)$$

where: p – thermodynamical pressure, $\mathbf{I} = \delta_{ij}\mathbf{e}_i \otimes \mathbf{e}_j$ – unit tensor, μ – dynamic viscosity, $\mathbf{d}$ – deformation rate tensor, $I_\mathbf{d} = d_{11} + d_{22} + d_{33}$ – the first invariant of the deformation rate tensor, R – gas constant, T – temperature.

2.2   The set of CSD balance equations

The problem of vibrations in constructions has been discussed in [27,28], the modal vibration and harmonic analysis used by the finite elements method (FEM) of discretization in [24] and the problem of the determination of the non-stationary load coming from wind flow is explained in [20].

The set of CSD (computational solid dynamics) governing equations has been created by analogy from the CFD set of governing equations in the Euler description as follows [6,26]:

$$\frac{\partial}{\partial t}\left\{\begin{array}{c} \rho \\ \rho\mathbf{v} \end{array}\right\} + \mathrm{div}\left\{\begin{array}{c} \rho\mathbf{v} \\ \rho\mathbf{v} \otimes \mathbf{v} \end{array}\right\} = \mathrm{div}\left\{\begin{array}{c} 0 \\ \boldsymbol{\sigma} \end{array}\right\} + \left\{\begin{array}{c} 0 \\ \rho\mathbf{b} \end{array}\right\}, \qquad (4)$$

where $\boldsymbol{\sigma}$ – Cauchy stress tensor. The mesh velocity $\mathbf{w}$ is not included in the CSD set of balance equations, therefore, the solid part has been simulated using FEM.

The stress and strain, calculated in CSD, will be expressed as second principal invariant of stresses and strains and with respect to the modal analysis the momentum balance expressed in a form useful to computational applications [6]

$$\mathbf{M}\ddot{\mathbf{q}}+\mathbf{K}q=\mathbf{F}^{\mathrm{ext}} \quad , \tag{5}$$

where $\mathbf{q}$ is the displacements vector, $\mathbf{F}^{\mathrm{ext}}$ is the excitation force matrix, and overdots represent the second time derivative. $\mathbf{M}$ and $\mathbf{K}$ are the mass matrix and stiffness matrix, respectively dependent on the Cauchy stress tensor $\boldsymbol{\sigma}$, respectively [8], defined as follows:

$$\mathbf{M} = \iiint\limits_{V_e} \mathbf{N}^\top \rho \mathbf{N} dV \ , \tag{6}$$

$$\mathbf{K} = \iiint\limits_{V_e} \left(\mathbf{N}^\top \mathbf{B}^\top \mathbf{D} \mathbf{B_{NL}} \mathbf{N} + \mathbf{N}^\top (\mathbf{B_{NL}})^\top \mathbf{D} \mathbf{B_{NL}} \mathbf{N} + \mathbf{N}^\top \mathbf{B_{NL}^\top} \mathbf{D} \mathbf{B} \mathbf{N} \right) dV \ , \tag{7}$$

where V_e is the volume of the solid element, $\mathbf{B}$ and $\mathbf{B}_{NL}$ are the linear and nonlinear strain-displacement transformations matrices, $\mathbf{D}$ is the material properties matrix, $\mathbf{N}$ is the shape function matrix, ρ is the density of the solid, and the symbol $\top$ denotes the transpose of a matrix [6].

3   Two dimensional CFD analysis

3.1   Description of 2D model used in validation process

At this point, the 2D case of laminar flow past a cylinder has been conducted in order to form a comparison with results presented in the literature. It is assumed that the cylinder is rigid and fixed and for this reason, within computational fluid dynamics set of equations for the 2D case, mesh velocity does not occur and the 2D model was discretized using a finite volume. The air flow characteristics of a circular cylinder in the 2D unsteady uniform cross flow are simulated numerically by means of the laminar model. This approach is justified by the fact that in the laminar model the vortices are not dissipated and therefore generate greater pressures on the mast surface, which gives a safety margin during the design process.

The 2D fluid domain used for the simulation (rectangular shape has dimensions 20 m×4 m) is shown in Fig. 1. The model, which contains 38098 quadrilateral finite volumes is presented in Fig. 2. Air properties are assumed as constant due to low variability in the environmental density (see Tab. 1). The following

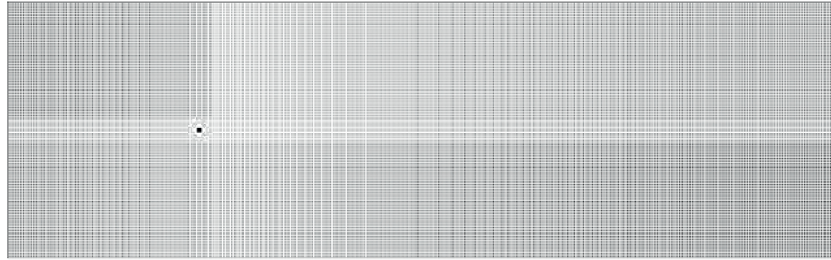Figure 1: Fluid 2D domain used for simulation.

Figure 2: Model discretization of the flow area.

Table 1: Air properties (at inlet).

Parameter	Unit	Value
Density	kg/m^3	1.225
Viscosity	kg/(m s)	1.7894×10^{-05}
Temperature	$^\circ$C	20
Pressure	Pa	101384
Gas constant	J/(mol K)	8.3144598(48)

boundary conditions are assigned in the model. The velocity on the external surface of the cylinder equals zero, as in [23] and is a typical condition applied at a wall. Velocity-inlet and outflow are correspondingly assigned to surfaces at the inlet and outlet of the domain. The lateral edges of the domain are treated as wall with full-slip conditions. In order to simplify the simulation, it is assumed that the upstream velocity is constant and uniform. Velocity at the inlet was calculated from Eq. (1), where $a = 0.1$ m (diameter of the mast), Sh = 0.18

(according to Tab. E.1. in [29] for a circular cross-section), $f = 16.68$ Hz. The f frequency was calculated for the geometry of the mast used for the purpose of FSI analysis, which is presented in the next paragraph. In consequence velocity at the inlet equals to 9.83 m/s.

4 Results of internally unsteady flow

In Fig. 3, static pressure for a time 30 s of simulation is shown. It can be observed that the highest value of pressure occurs on the leading side of air flow against the mast, which stays constant for the duration of the simulation. On the trailing side of the mast the static pressure has a negative value. The minimum value of static pressure oscillates alternately depending on time on the trailing side of mast.

Contour of static pressure [Pa] (time = 30 s)
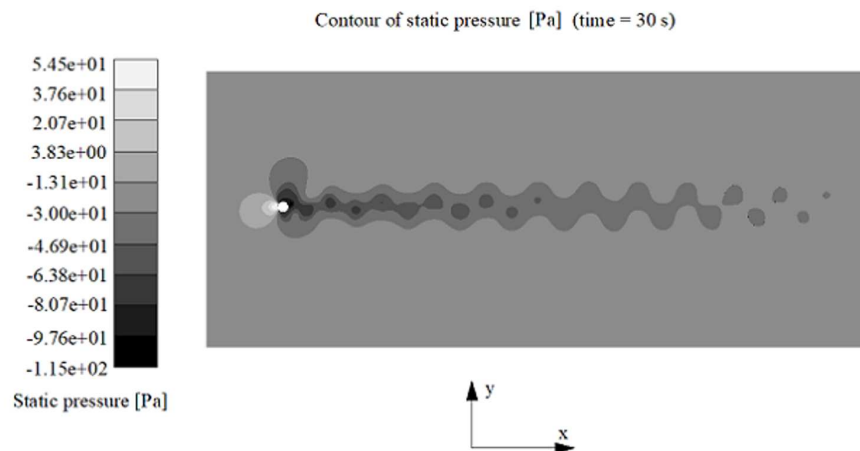
Figure 3: Static pressure in 30 second of simulation.

The frequency of the set vortices is independent of air properties and is dependent on flow velocity. In Fig. 4, the velocity magnitude for the 30 s of simulation of the mast area is shown. The flow behind the mast is vortical and asymmetrical and the so called Bénard-Kàrmàn vortices occur. The vortices form alternately.
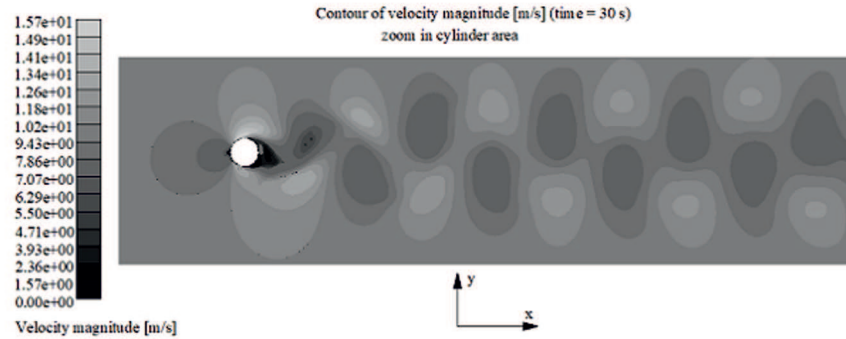
Figure 4: Velocity magnitude in 30 second of simulation.

5 Discussion and comparison with the literature

In Fig. 5 the distances between the vortices are shown and are compared to the distances from Fig. 6, where the flow past cylinder in the subcritical range is presented [1]
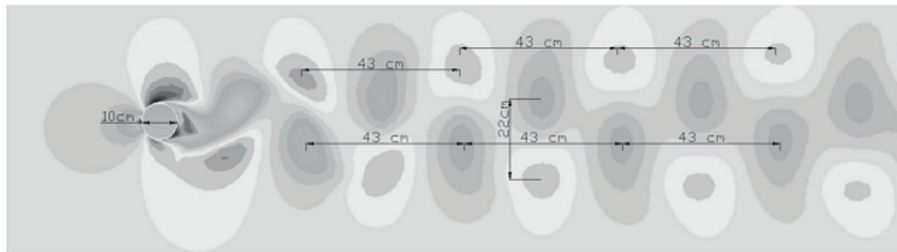

Figure 5: The distances between the vortices.

According to Flaga [1] the distance, l, between the two neighboring vortices is approximately $l \approx 4.3D$ ($D = 0.1$ m – diameter of the mast) which is consistent with a distance of approximately 0.43 m. The distance between the two rows of vortices, h, in most cases is equal to $h \approx 0.28l$, but the range is between 0.25–0.53. In the case of this simulation it is equal to $22/43 = 0.51$ and is within the range given in [1].

In order to check the validity of the results the Strouhal number obtained in the present paper for 2D simulation was marked on the diagram of the Strouhal-Reynolds Number relationship for circular cylinders (Fig. 7), taken from [30]. It is worth mentioning that the diagram in Fig. 7 has been created as a result of
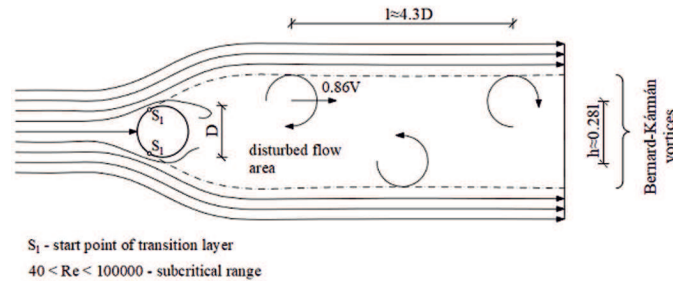
Figure 6: The flow past cylinder in the subcritical range [1].

experiments on rigid circular cylinder [31] and the sketch consists of the major regimes of interest for the entire range of Reynolds numbers, Re. It should be noted that periodicity of the vortex street vanishes at a distance of circa 48 diameters downstream from the cylinder according to [30] and this is also observed in the current analysis.
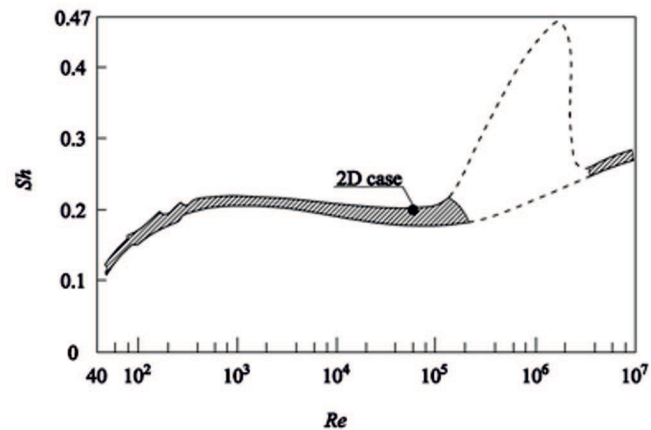

Figure 7: Comparison of Sh vs. Re from [30] to 2D results.

6 FSI analysis

In this section the two-way fluid structure interaction analysis is conducted using the partitioned method. The model contains a fluid part – air (air properties are available in Tab. 1.) and a solid part – a mast (refer to Tab. 2 for the mast material

properties). Visualization of the domain geometry and the assigned boundary conditions is shown in Fig. 8. The response of the mass in the calculations is assumed to be linear and elastic.

Table 2: Mast steel properties.

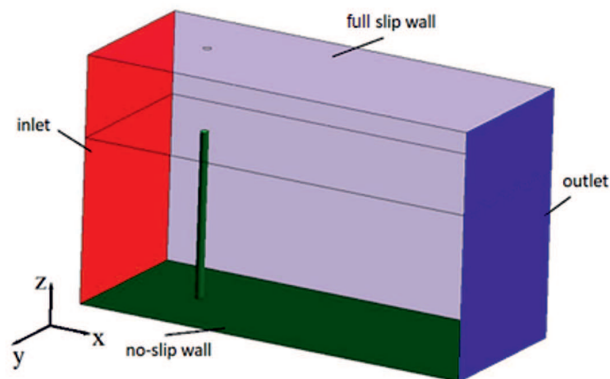| Parameter	Unit	Value
Density	kg/m^3	7850
Coefficient of thermal expansion	1/$^\circ$C	1.2×10^{-05}
Young's modulus	GPa	200
Poisson's ratio	–	0.3
Tensile/compressive yield strength	MPa	250
Tensile ultimate strength	MPa	460

Figure 8: Boundary conditions – inlet, outlet no-slip wall and full-slip wall.

The mast is divided into 603 finite elements (20-nodal hexahedral elements – SOLID186). The air domain was divided into 1146949 finite volumes (8-nodal hexahedral volumes – FLUID30) using the cut cell method. A description of the cut cell method can be found in [32–33].
The inlet and outlet conditions are the same as in the 2D case. The top surface and lateral surfaces are treated as full-slip walls, while the bottom surface and side surface of the mast are no-slip walls. The simulation is performed for the time period of 5 s.

In Figs. 9 and 10, the horizontal and vertical cross-sections with distributions of the velocity in the y-direction (cross-stream) are presented. Vortices form
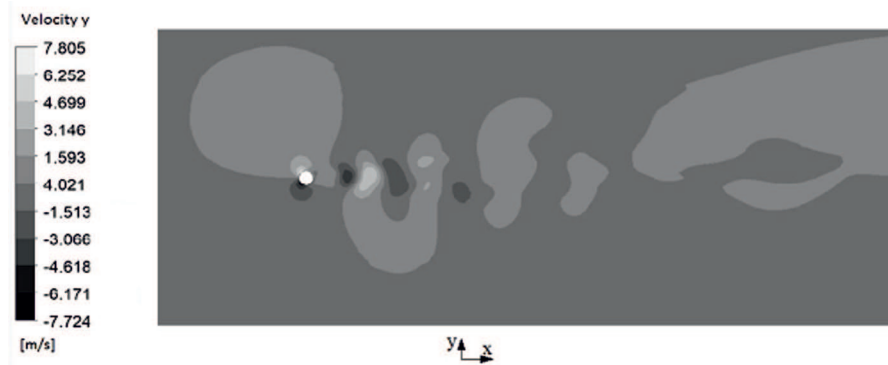

Figure 9: Distribution of velocity in y-cross-stream direction (horizontal cross-section) in 5 seconds of simulation.
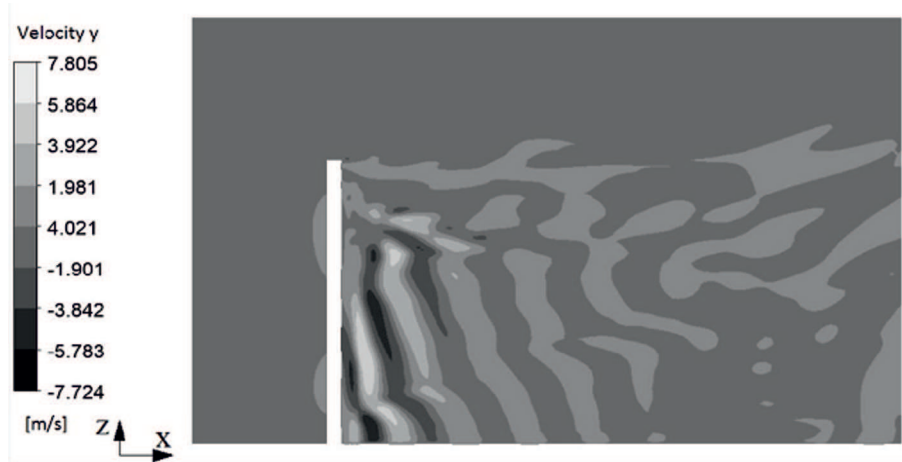

Figure 10: Distribution of velocity the y-cross-stream direction (vertical cross-section) in 5 second of simulation.

alternately as in the 2D case, however, they disappear more rapidly. Figure 10 clearly illustrates the oscillations of the air flow. It can be observed that the value of the velocity changes from positive to negative. It is also noteworthy that the vortices form in different phases at different heights behind the mast. The boundary layer flow around the base of the mast, the flow over the free end and the oscillations of the mast cause distinct changes in the flow pattern along the

cylinder height. Parallel eddy filaments have formed only at the lower part of the mast. Thus, the wake on the leeward side of the flow is more complex than in the 2D case.

Air velocities in the y-direction (cross-stream direction) also differ at different height levels, (1 m, 1.5 m, and 2 m). This is portrayed for the points located at aforesaid height levels and at a distance of 0.1 m behind the mast in Fig. 11. The amplitude of the cross-stream velocity oscillates with visible peaks.

The velocity at the mast in the y-cross-stream direction at a point at the top of the mast during the 5 second of the simulation is presented in Fig. 12. It is observed that the amplitude of the velocity starts to decrease and increase alternately as in the beat phenomenon [34]. The initial phase of the simulation is characterized by the low values of the velocity amplitudes. After 2 s, the amplitudes increased several times.
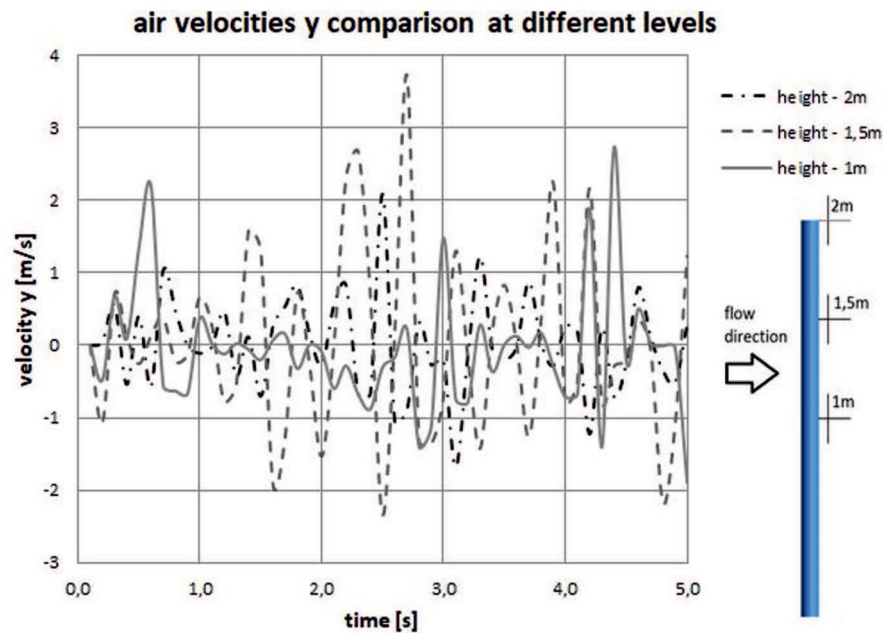

Figure 11: Air flow velocities in the y-cross-stream direction at 3 different levels at a distance of 0.1 m behind the mast.
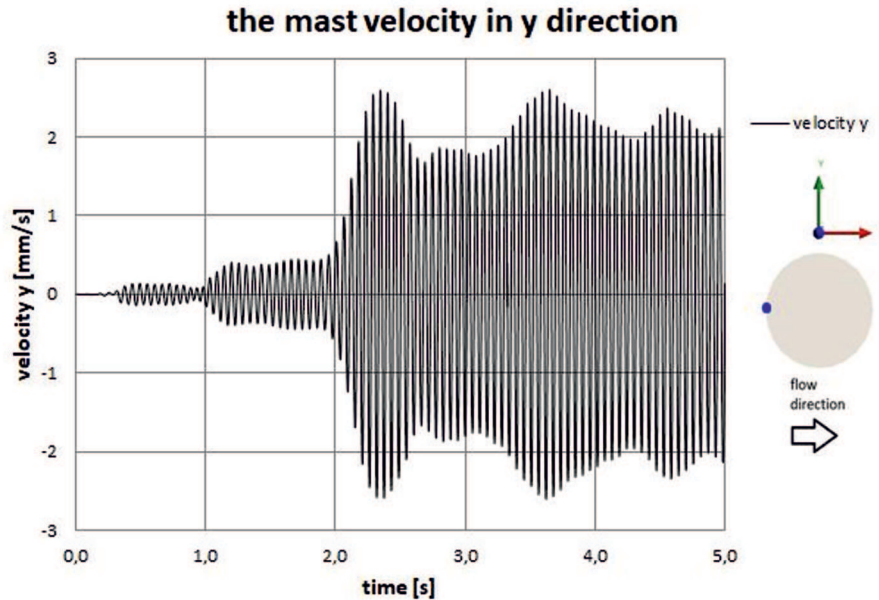
Figure 12: The mast velocity in the y-cross-stream direction at point at the top during the time interval 0–5 s of simulation.

7 Unsteady forces

The resultant force and the components of the resultant force in the mast, arising due to unsteady pressures acting on the mast, are shown in Fig. 13. The force resultant can be defined as

$$\text{Force resultant} = -\iint p\mathbf{n}dA \; , \tag{8}$$

where p is the unsteady pressures acting on the mast, $\mathbf{n}$ – vector normal to the surface of the mast, and A – surface area of the mast.

The force resultant can also be written as a square root of the sum of the squares of the components:

$$\text{force resultant} = \\ \sqrt{[\text{force resultant(X)}]^2 + [\text{force resultant(Y)}]^2 + [\text{force resultant(Z)}]^2} \; . \tag{9}$$

The force resultant (X) can be understood as a drag force obtained numerically and the force resultant (Y) as the lift force. It should be noted that the force

resultant (Z), aside from the initial phase of the simulation, has maintained a constant value and is very low, as the wind action in the longitudinal direction of the mast is small compared to the remaining directions X and Y. The force resultant (X) values have started to oscillate around a slightly changing value after about 2.5 s. Although the force resultant (X) has the highest value of force, the force resultant (Y) has the highest amplitude. This suggests that the forces in the mast have very unsteady characteristics.
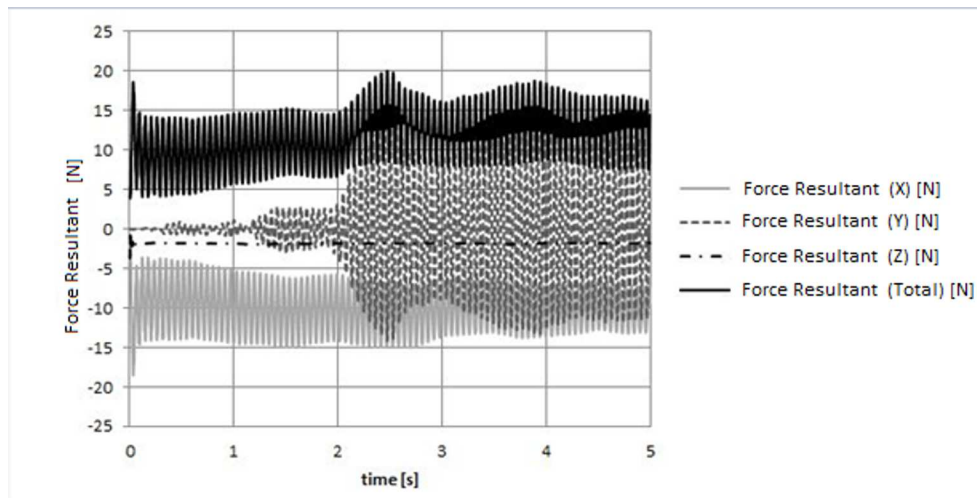

Figure 13: The resultant force and components of the resultant force due to unsteady pressures acting on the mast.

8   Conclusions

Firstly, a 2D simulation of Bernard-Kármán vortex shedding formation phenomenon has been conducted. The results of this 2D simulation, particularly the distances between two neighboring vortices and two rows of vortices, are in agreement with the literature sources.

As the 2D calculations validated the approach, a two-way fluid structure interaction analysis has been performed for a mast immersed in a flow. In consequence, the mast vibrations have been induced and vortices started to shed from the body. The eddy filaments have formed only at the lower part of the mast. The observed air flow behavior is different at different height levels behind the mast. Vortices behind the mast form alternately and in the 3D simulation they disappear quicker than in the 2D analysis. The amplitude of velocity at the

point lying at the top of the cylinder increased significantly after 2 s of the flow. The transverse and streamwise oscillations of the mast cause changes in the flow pattern of the boundary layer around the base of the mast, along the cylinder height and in the vicinity of the free end. The wake formed behind the mast structure is thus complex. The differences between 2D and 3D results presented and discussed within this paper demonstrate the complexity of the phenomena. The changes in resultant force and its components that induce mast deformations, suggest that the forces in the mast are unsteady as well.

Received in April 2017

References

[1] Flaga A.: *Wind Engineering. Basics and Applications.* Arkady, Warszawa 2008 (in Polish).

[2] Simiu E., Scanlan R.H.: *Wind Effects on Structures: Fundamentals and Applications to Design.* John Wiley & Sons Inc., 1996.

[3] Wilde K.: *Passive Aerodynamic Control of Wind Induced Instabilities in Long Span Bridges.* GUT Press, Gdańsk 2002.

[4] Strouhal V.: *Uber eine besondere art der tonerregung.* Ann. Physik Chemie. Neue Folge **5**(1878), 126–251.

[5] Shyy W.: *Computational Modeling for Fluid Flow and Interfacial Transport.* Dover Pub., New York 1994.

[6] Kornet S., Sławiński D., Ziółkowski P., Badur J.: *Analysis of unsteady flow forces on the thermowell of steam temperature sensor.* Trans. Inst. Fluid-Flow Mach. **129**(2015), 25–49.

[7] Saha A.K.: *Three-dimensional numerical study of flow and heat transfer from a cube placed in a uniform flow.* Int. J. Heat Fluid Flow **26**(2006), 80–94.

[8] Sarpkaya T.: *A critical review of the intrinsic nature of vortex-induced vibrations.* J. Fluid Struct. **19**(2004), 389–447.

[9] Baarholm G.S, Larsen C.M, Lie H.: *On fatigue damage accumulation from in-line and cross-flow vortex-induced vibrations on risers.* J. Fluid Struc. **22**(2006), 109-127.

[10] Sobczyk B., Chróścielewski J., Witkowski W.: *Wind induced vibration analysis of composite footbridge.* Biul. WAT **64**(2015), 1, 91–101 (in Polish).

[11] Dettmer W.G., Perić D.: *On the coupling between fluid flow and mesh motion in the modeling of fluid-structure interaction.* Comp. Mech. **43**(2008), 81–90.

[12] Wilde K., Witkowski W.: *Simple model of rain-wind-induced vibrations of stayed cables.* J. Wind Eng. Ind. Aerod. **91**(2003), 873–891.

[13] Goujon-Durand S., Jenffer P., Wesfreid J.E.: *Downstream evolution of the Benard-von Kármán instability.* Phys. Rev. E. **50**(1994), 1, 308–315.

[14] Zarruk G.A., Cowen E.A., Wu T.-R., Liu P.L-F.: *Vortex shedding and evolution induced by a solitary wave propagating over a submerged cylindrical structure.* J. Fluid Struc. **52**(2015), 181–198.

[15] Norberg C.: *Fluctuating lift on a circular cylinder: review and new measurements.* J. Fluid Struc. **17**(2003), 57–96.

[16] Zdravkovich M.M.: *Flow Around Circular Cylinders: Vol. 1. Fundamentals.* Oxford University Press, Oxford 1997.

[17] Sumner D.: *Flow above the free end of a surface-mounted finite-height circular cylinder: A review.* J. Fluids Struc. **43**(2013), 41–63.

[18] Piperno S., Farhat C., Larrouturou B.: *Partitioned procedures for the transient solution of coupled aeroelastic problems. Part I: Model problem, theory and two dimensional application.* Comput. Meth. Appl. M. **124**(1995), 1-2, 79–112.

[19] Farhat C., Lesoinne M., Maman N.: *Mixed explicit/implicit time integration of coupled aeroelastic problems: there-field formulation, geometric conservation and distributed solution.* Int. J. Numer. Meth. Fl. **21**(1995), 10, 807–835.

[20] Fahrat C., Lesoinne M.: *Two efficient staggered algorithms for the serial and parallel solution of three-dimensional nonlinear transient aeroelastic problems.* Comput. Method. Appl. M.**182**(2000), 499–515.

[21] Fahrat C., Van der Zee K.G., Geuzaine P.: *Provably second-order time accurate loosely-coupled solution algorithms for transient nonlinear computational aeroelasticity.* Comput. Meth. Appl. M. **195**(2006), 1973-2001.

[22] Vaze M., Haiyan M., Gopalan H., Joo P.H., Jing L.: *Methodology Development for Wind Driven Cantiliver Vibration using Fluent-Structural Interaction.* In: Proc. World Cong. Computational Mechanics XII, Seoul, July 2016.

[23] Badur J.: *Numerical modeling of sustainable combustion in gas turbine.* Rep. IMP PAN, Gdańsk 2003 (in Polish).

[24] Zienkiewicz O.C.: *Finite Element Method: Vol. I, II, III.* Elsevier 2005.

[25] Hou G., Wang J., Layton A.: *Numerical methods for fluid-structure interaction – A review.* Commun. Comput. Phys. **12**(2012), 2, 337–377.

[26] Badur J.: *Five lectures of Contemporary Fluid Thermomechanical Fluids* (2nd Edn.) Wyd. IMP PAN, Gdańsk 2005 (in Polish).

[27] Chopra A.K.: *Dynamics of Structures: Theory and Applications to Earthquake Engineering.* Prentice Hall, New Jersey 1995.

[28] Rucka M., Wilde K.: *Structural Dynamics with Examples in Matlab.* GUT Press, Gdańsk 2011 (in Polish).

[29] Eurocode 1: Actions on structures – General actions – P. 1-4: Wind actions (EN 1991-1-4:2004).

[30] Lienhard J.H.: *Synopsis of Lift, Drag and Vortex Frequency Data for Rigid Circular Cylinders.* Washington State University, College of Engineering, Res. Div. Bull. **300**(1966), 1–32.

[31] Blevins R.D.: *Flow-induced vibration.* Krieger Publishing Company, Malabar 1986.

[32] Tucker P.G., Pan Z.: *A Cartesian cut cell method for incompressible viscous flow.* Appl. Math. Model. **24**(2000), 591–606.

[33] Ingram D.M., Causon D.M., Mingham C.G.: *Developments in Cartesian cut cell methods.* Math. Comput Simulat. **61**(2003), 561–572.

[34] Skorko M.: *Physics.* PWN, Warszawa 1978 (in Polish).